J Mater Sci (2010) 45:3080–3087
DOI 10.1007/s10853-010-4315-9

Effect of aluminum on precipitation hardening in Cu–Ni–Zn alloys

Xiao-Zhong Zhou · Yu-Chang Su · Jin-Ming Sun

Received: 16 October 2009 / Accepted: 10 February 2010 / Published online: 23 February 2010

Abstract The effect of aluminum on the precipitation hardening of Cu–Ni–Zn alloys with varying aging temperatures and times was investigated in this article, in the hope to achieve better mechanical properties. Vickers hardness, tensile, and electrical conductivity tests were carried out to characterize the properties of the Cu–Ni–Zn alloys with or without an addition of aluminum subjected to different aging treatments. The results show that an addition of 1.2 wt% aluminum can play an influential role in the precipitation hardening of the Cu–Ni–Zn alloys. For example, it can increase the peak hardness from 58 Hv for the solution-treated Cu–10Ni–20Zn alloy to 185 Hv for the solution-treated Cu–10Ni–20Zn–1.2Al alloy during aging at 500 °C. The yield strength, tensile strength, and electrical conductivity of the Cu–10Ni–20Zn–1.2Al alloy subjected to suitable treatments under prior cold-rolled and aged conditions can reach 889 MPa, 918 MPa, and 10.96% IACS, respectively, being much higher than those of the relevant alloy without aluminum and comparable to those of the Cu–Be alloys (C17200 and C17510). According to the transmission electron microscope observations, it was found that formation of nanosized precipitates with the $L1_2$-type ordered lattice results in precipitation hardening, and an orientation relationship of $[011]_p//[011]_m$ and $(100)_p//(200)_m$ exists between the precipitates and the α-Cu matrix.

X.-Z. Zhou · Y.-C. Su (✉) · J.-M. Sun
School of Materials Science and Engineering,
Central South University, Changsha 410083,
Hunan, People's Republic of China
e-mail: ychsu@mail.csu.edu.cn

Introduction

The Cu–Ni–Zn alloys have found extensive applications in marine fittings and plumbing fixtures due to their corrosion resistance, in heating coils due to their high electrical resistance, and in computer industry due to their high thermal conductivity [1]. One of the most prominent applications of the Cu–Ni–Zn alloys is to use them as spring materials in electromechanical relays or in electronic device packages. Current efforts focused on devising miniature relays and device assemblies have resulted in higher stresses on the spring components, and hence there is a need for increased strength of the Cu–Ni–Zn alloys.

Up till now, several methods, such as grain size strengthening [2], have been used to improve the strength of the Cu–Ni–Zn alloys. However, tensile strength and electrical conductivity are incompatible characteristics. When the tensile strength is increased with heavy cold forming like rolling, electrical conductivity slightly falls. In case of strengthening with the precipitation hardening, both the tensile strength and electrical conductivity can be improved simultaneously. Therefore, the effect of precipitation hardening might be achieved by adding a fourth component, for example aluminum, though Cu–Ni–Zn alloys containing less than 28 wt% Zn form only solid solutions. Introducing aluminum to Cu–Ni alloys can improve their strength due to precipitation hardening [3, 4], but few articles have been published concerning the precipitation hardening in Cu–Ni–Zn alloys with a small addition of aluminum. Several articles on quaternary Cu–Zn–Al–Ni alloys have been published [5–7]. However, these studies are focused on small additions of nickel into ternary Cu–Zn–Al alloys to improve shape memory effect, making it suitable for practical applications, and their aluminum content was higher than 3.8 wt%.

To our knowledge, an authentic phase diagram of the Cu–Ni–Zn–Al quaternary system has not been available right now, but a ternary phase diagram of the Cu–Ni–Al system at 500 °C [8] shows that the Cu–Ni–Al alloys containing ca. 10 wt% Ni and ca. 1.2–3.0 wt% Al falls in the region of Cu solid solution and Ni_3Al phase at equilibrium. To achieve better properties a modified Cu–10Ni–20Zn alloy with small additions of aluminum (1.2 wt%) was designed in the present work, and a detailed study was then undertaken to investigate the precipitation hardening behavior of the Cu–10Ni–20Zn–1.2Al (wt%) alloy. The findings of this study are presented herein.

Materials and methods

Material and specimen preparation

The nominal composition of two alloys investigated in this work was Cu–10Ni–20Zn and Cu–10Ni–20Zn–1.2Al, respectively. The two alloys were prepared in an induction furnace under air atmosphere using 99.99% copper, 99.9% zinc, 99.99% nickel, and 99.99% aluminum as the starting materials. Results from chemical analysis indicated that the final alloy composition is close to the nominal one. The raw materials were melted and chill cast into a 25 mm × 120 mm × 200 mm water-cooled iron crucible. To improve their mechanical properties and to break up their coarse casting microstructure, the cast ingots were homogenized at 850 °C for 12 h, and then hot rolled down to 6.0 mm in thickness. After that, the hot-rolled sheets were solution treated at 925 °C for 60 min followed by water-quenching, and then cold rolled to 80% reduction. Several flat square specimens were obtained from the solution-treated sheets and the cold-rolled sheets. To investigate the difference in the properties of the Cu alloy with and without aluminum during aging, both the solution-treated alloys Cu–10Ni–20Zn and Cu–10Ni–20Zn–1.2Al were isothermally aged at 500 °C. As well known, cold rolling can accelerate the aging process, so the cold-rolled alloys were isothermally aged at a relatively lower temperature, 450 °C, to be better investigating the effect of Al addition on precipitation hardening after cold rolling. To investigate the effect of temperature on the precipitation hardening behavior, the specimens from the cold-rolled Cu–10Ni–20Zn–1.2Al alloy with 80% reduction were isothermally aged at 350, 400, 450, and 500 °C. Surface oxide layers on the specimens were removed by machining.

Mechanical properties and microstructural features

Vickers hardness and tensile properties were measured to analyze the mechanical properties of both the alloys using flat specimens under different conditions. The Vickers hardness was measured under an indenting load of 2 kg on the mechanically polished sections of the specimens. To ensure accuracy of the results, the mean value of five indentations was taken as the hardness of the corresponding condition. The tensile testing specimens have a thickness of 1 mm, a width of 10 mm, and a gage length of 65 mm with their longitudinal directions parallel to the rolling direction. They were ground and polished after machining. Two tests were performed for each condition. The tensile tests were conducted at a crosshead speed of 2 mm/min at room temperature in air with an MTS 810 material testing system. Values of tensile strength and 0.2%-offset yield strength were then calculated for each sample.

Electrical conductivity (EC) was evaluated using international annealed Cu standard (IACS). The electrical resistance was determined by measuring the resistance of specimens in 100-mm length using Double-Arm Electrical Bridge apparatus at room temperature in solution-treated (ST), ST + aged and ST + cold-rolled + aged conditions, according to the ASTM B193-02 specification, using the following expressions:

$$\rho = (R \cdot A)/L \quad (1)$$

$$\mathrm{EC} = 172.41/\rho \quad (2)$$

where ρ, R, L, and A are the resistivity (μΩ cm), the resistance (μΩ), the length (cm), and the cross-sectional area (cm^2) of the sheets, respectively.

Microstructure of the alloys was observed by optical microscope (OM). Structure and morphology of the precipitate phase were characterized by Tecnai G^2 20 transmission electron microscope (TEM) operated at 200 kV. For OM observation, the specimens were mechanically polished until a mirror-like surface was obtained, and then etched with a solution of 2 g $Fe(NO)_3$ dissolved into 50 mL CH_3COOH. For TEM observation, specimens that were cut from isothermally aged sheets of the Cu–10Ni–20Zn–1.2Al alloy were prepared using ion milling technique. After being ground manually from both sides down to a final thickness of ca. 80 μm using SiC paper (grade p 1400), the 3 mm discs were punched from these thick foils, and then dimpled grinding in a Gatan 656 Dimple Grinder to a residual thickness of 15 μm. After dimpling, the samples were ion beam polished to generate a large electron transparent area using a Gatan Model 691 Precision Ion Polishing System (PIPS) instrument. Directional milling was used to eliminate milling the aluminum stubs. This was accomplished by turning the ion guns on and off during the sample rotation. The double-sided milling was used, where the left gun was tilted 7° from the top of sample and the right gun was tilted 5° from the bottom of sample. The voltage of ion beam was kept at 5.0 kV until

the sample was perforated. When the perforation was detected, the voltage of ion beam was reduced to 2.5 kV and then held for 15 min, where the left gun was tilted 4° from the top sample and the right gun was tilted 2° from the bottom of sample. Subsequently, the voltage was reduced to 2.0 kV again and then held for another 15 min. In order to prevent overheating, a repeated milling process was interrupted at intervals of 10 min so that the samples will be cooled to room temperature.

The variation of dislocation density in the cold-rolled alloy with aging time at 450 °C were characterized by examining the change in the full width at half maximum (FWHM) of X-ray diffraction peaks at room temperature. The X-ray diffraction (XRD) pattern was carried out on the mechanically polished specimens using a D/Max-2500 X-ray powder diffractometer with CuKα radiation at a step size of 0.02° and counting time of 0.6 s/step. All the diffraction peaks were fitted by a pseudo-Voigt (pv) function.

Results and discussion

Age-hardening behavior

The variations of the Vickers hardness and electrical conductivity of the solution-treated Cu–10Ni–20Zn–1.2Al alloy and the ternary Cu–10Ni–20Zn alloy with the aging time at 500 °C are shown in Fig. 1. The Vickers hardness of the un-aged alloys (Fig. 1a) shows that the alloy with aluminum has a slightly higher value but the difference between these two Cu alloys is not significant. However, both the Cu alloys have different tendencies in the variations of hardness with aging time. It is interesting to find that the solution-treated Cu–10Ni–20Zn–1.2Al alloy exhibits an age-hardening response, whereas the solution-treated Cu–10Ni–20Zn alloy exhibits no age-hardening response. During the aging at 500 °C, the Vickers hardness (Hv) of the solution-treated Cu–10Ni–20Zn–1.2Al alloy increases continuously as a function of aging time before reaching its peak hardness. It rose rapidly during the first 0.5 h and kept increasing during the following 16 h until a peak value of 185 Hv was reached. After reaching the peak value, the Vickers hardness was held stable over a relatively long range and then gradually decreased as a result of over aging. The quenched hardness of the Cu–10Ni–20Zn–1.2Al alloy is 65 Hv, and thus the hardness due to age hardening is 120 Hv. Therefore, it is evident that an addition of 1.2 wt% aluminum to the Cu–10Ni–20Zn alloy results in a considerable age-hardening response and a great increase in hardness. From Fig. 1b, it can be observed that, with increase in aging time, the electrical conductivity of the Cu–10Ni–20Zn alloy shows a stable value of ca. 9.5% IACS with aging time, while the electrical conductivity of the Cu–10Ni–20Zn–1.2Al alloy increases substantially with the increase of the isothermal aging time. The electrical conductivity of the Cu–10Ni–20Zn–1.2Al alloy increases rapidly at early stage of aging, because the high density of the lattice defects facilitated occurrence of the precipitate phase out of the supersaturated matrix. As the aging time increases, the degree of supersaturation decreases, the velocity of precipitation slows, and the ratio of the electrical conductivity increase lessens. The longer the time, the more precipitates occur. The growth of precipitates reduces the contents of solute atom in matrix and results in a continuous increase in electrical conductivity during the aging, and a value as high as 11.67% IACS was obtained after aging for 128 h, indicating that an addition of 1.2 wt% aluminum to the Cu–10Ni–20Zn alloy also increases its electrical conductivity.

Cold work prior to aging increases the hardness considerably in the solution-treated condition. Figure 2 shows the variations of the Vickers hardness and electrical

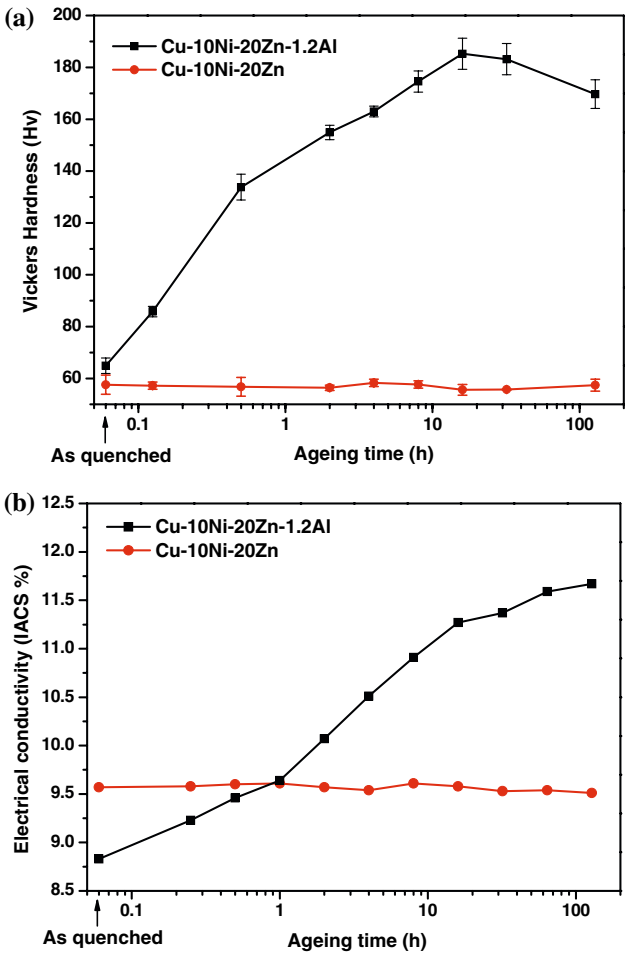

Fig. 1 Variations of the Vickers hardness (**a**) and the electrical conductivity (**b**) of the solution-treated Cu–10Ni–20Zn–1.2Al alloy and the ternary Cu–10Ni–20Zn alloy with ageing time at 500 °C

conductivity of the cold-rolled Cu alloys with 80% reduction during isothermal aging at 450 °C with the aging time. The increases in hardness for both the alloys after cold rolling can be attributed to the great effect of the dislocation networks formed during the deformation process. For Cu–10Ni–20Zn–1.2Al alloy, achieving the peak hardness can be accelerated using cold rolling prior to the isothermal aging. For example, the aging time required to attain the peak hardness for the Cu–10Ni–20Zn–1.2Al alloy is 4 h with 80% cold rolling, which is 75% less than that required for the isothermal aging at 500 °C without cold rolling. This indicates that the cold deformation not only reduces the peak aging temperature, but also shortens the peak aging time. Because aluminum is in a super-saturated solid solution state and the specimens are subjected to an extensive deformation, the associated aging kinetics were accelerated, thus giving rise to a maximum hardness at a shorter aging time and promoting precipitation of a very fine metastable phase in increased volume fraction. Cold rolling prior to aging also accelerates the increase of the electrical conductivity, as shown in Fig. 2b. The electrical conductivity decreases slightly after cold rolling due to the dislocations resulting from cold rolling, which can increase the scattering probability of electrons. It can be seen that the electrical conductivity of the cold-rolled Cu–10Ni–20Zn–1.2Al alloy increases substantially with the increase of the isothermal aging time, and a value of 11.79% IACS was obtained after aging at for 128 h. The accelerated increase in electrical conductivity and the accelerated age hardening after cold rolling can be attributed to a higher rate of precipitation resulting from the presence of dislocations, which are believed to be favorable sites for formation of nuclei [9]. However, for the cold-rolled Cu–10Ni–20Zn alloy, the Vickers hardness gradually decreases with aging time and the increase in hardness or electrical conductivity is never observed (Fig. 2).

Figure 3 shows the evolution of the Vickers hardness of the cold-rolled Cu–10Ni–20Zn–1.2Al alloy with 80% reduction during the isothermal aging at 350, 400, 450, and 500 °C. For the cold-rolled Cu–10Ni–20Zn–1.2Al alloy, the peak hardness cannot be reached by aging at 350 °C even after 152 h. The highest hardness was ca. 269 Hv after cold rolling and aging at 400 °C for 64 h, beyond which it will decrease with the aging time. At 450 °C, the peak hardness is found to be slightly lower, i.e., 266 Hv for 4 h, but the over aging is faster. The peak hardness is lower than that at 450 °C, and the over aging is drastic on aging at 500 °C. On the other hand, for the age-hardening alloy, the time to obtain the peak hardness decreases with increasing the aging temperature. It takes about 64, 4, and 1 h to obtain the peak hardness of the Cu–10Ni–20Zn–2Al alloy aged at 400, 450, and 500 °C, respectively. The highest hardness, i.e., 269 Hv, is observed for the alloy

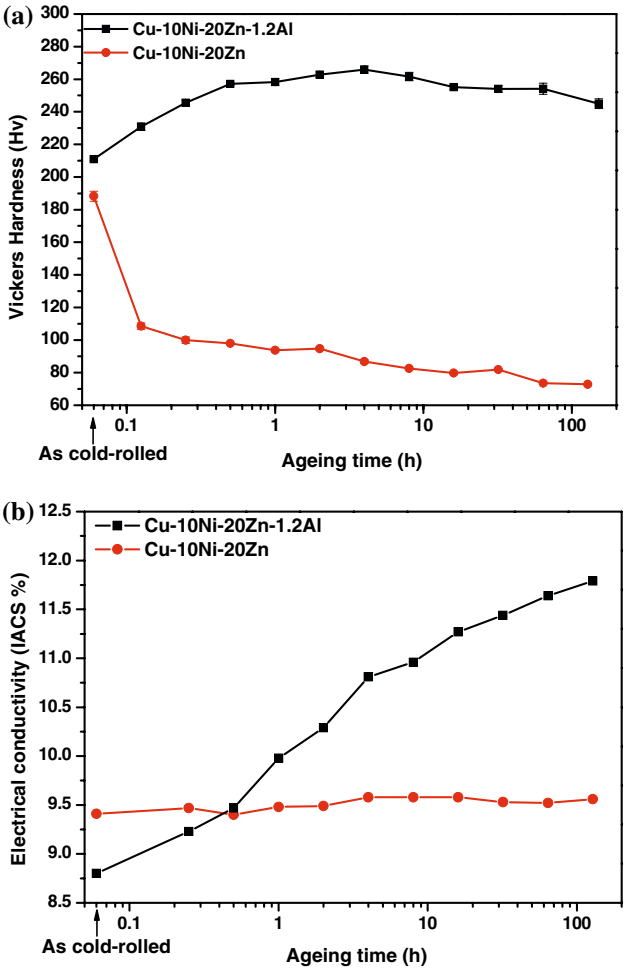

Fig. 2 Variations of the Vickers hardness (**a**) and the electrical conductivity (**b**) of the cold-rolled Cu–10Ni–20Zn–1.2Al alloy and the ternary Cu–10Ni–20Zn alloy with ageing time at 450 °C

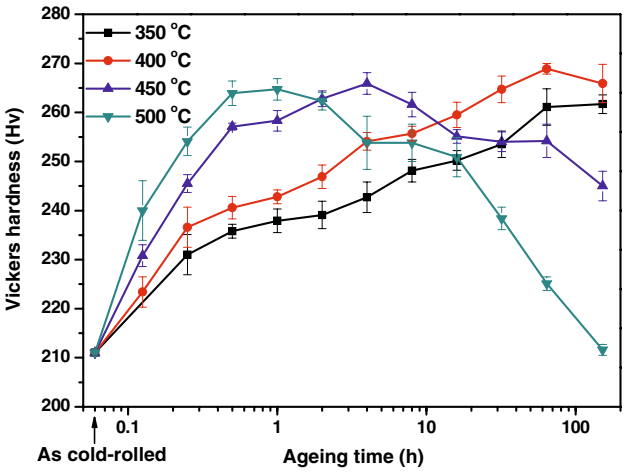

Fig. 3 Hardening curves of the cold-rolled Cu–10Ni–20Zn–1.2Al alloy with 80% reduction aged at different temperatures

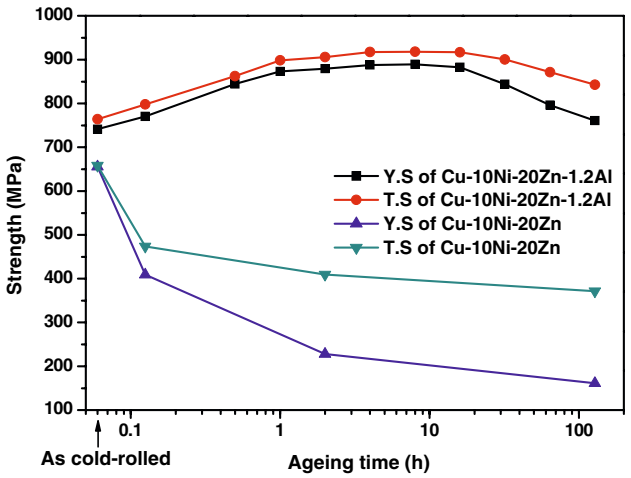

Fig. 4 Variations of the tensile properties of the cold-rolled Cu–10Ni–20Zn–1.2Al alloy and the Cu–10Ni–20Zn alloy during isothermal aging at 450 °C

aged at 400 °C for 64 h. The higher the temperature of aging, the smaller the effect is.

The variations of the tensile properties of the alloys with and without aluminum after 80% reduction during the isothermal aging at 450 °C are shown in Fig. 4. It can be seen that the Cu–10Ni–20Zn alloy exhibits an inferior tensile strength compared to the relevant alloy with aluminum addition, and its strength decreases rapidly with increasing the isothermal aging time due to recrystallization. However, both the yield strength (YS) and the tensile strength (TS) are obviously improved with an addition of 1.2 wt% aluminum. The trends in the evolution of the yield and tensile strengths during the aging for the Cu–10Ni–20Zn–1.2Al alloy are generally consistent with the observations of the hardness development during the aging at 450 °C (Fig. 3). The Cu–10Ni–20Zn–1.2Al alloy shows the highest yield and tensile strengths after aging at 450 °C for 8 h, and the relevant values are 889 and 918 MPa, respectively, while the corresponding electrical conductivity reaches 10.96% IACS (Fig. 2b), being 1.36 times higher than those of the Cu–10Ni–20Zn alloy. It is found that the mechanical properties of the Cu–10Ni–20Zn–1.2Al alloy in prior cold worked and aged condition can be comparable to those of the Cu–Be alloys (C17200 and C17510) [1] and the Cu–2.7Ti alloy [10].

Microstructure analysis

The Cu–10Ni–20Zn–1.2Al alloy shows a visible age-hardening response during the aging treatments. Therefore, in order to understand the response of the mechanical properties to aging, the microstructural changes resulting from aging are characterized on the Cu–10Ni–20Zn–1.2Al alloy with the helps of the OM and TEM characterizations.

Figure 5a–c illustrates the optical microstructures of the Cu–10Ni–20Zn–1.2Al alloy in the solution treated, peak aged, or over-aged conditions, respectively. The microstructures are identified by the presence of equiaxed grains with annealing twins. With the increase of the aging time, more and more round precipitate particles can be observed

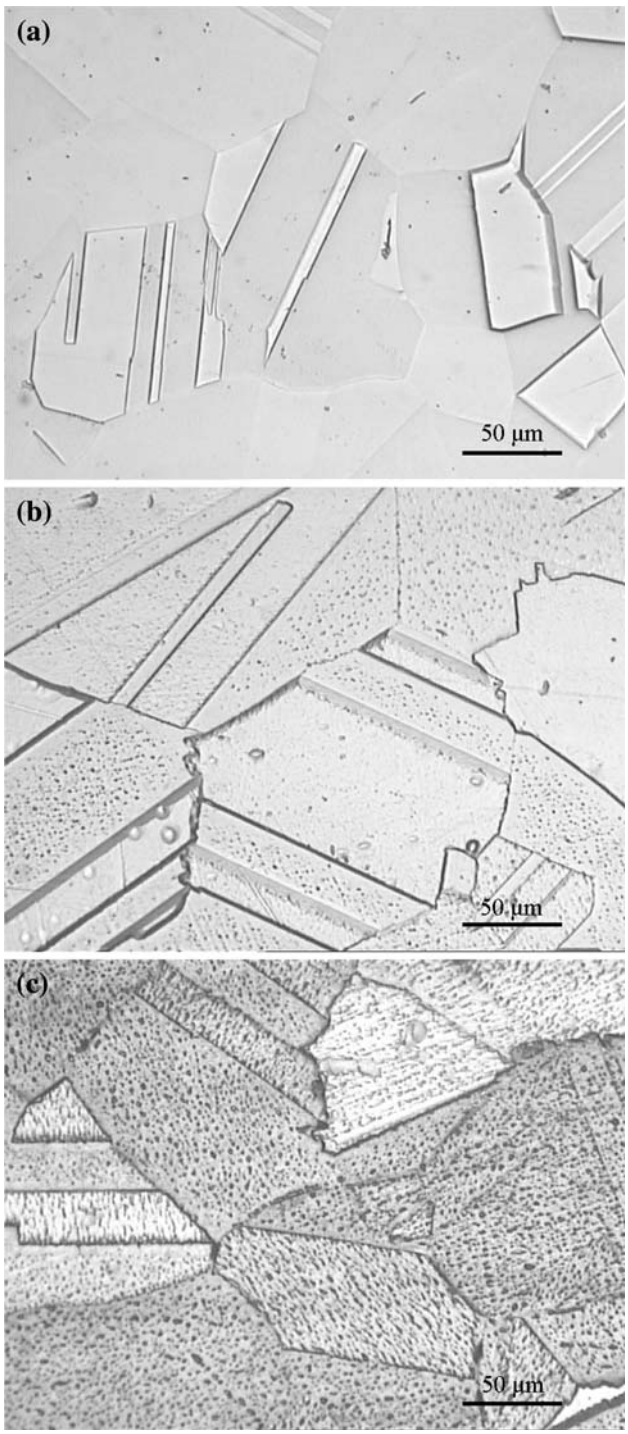

Fig. 5 Optical micrographs of the Cu–10Ni–20Zn–1.2Al alloy under solution treated (**a**), peak aged (**b**), and over aged (**c**) conditions

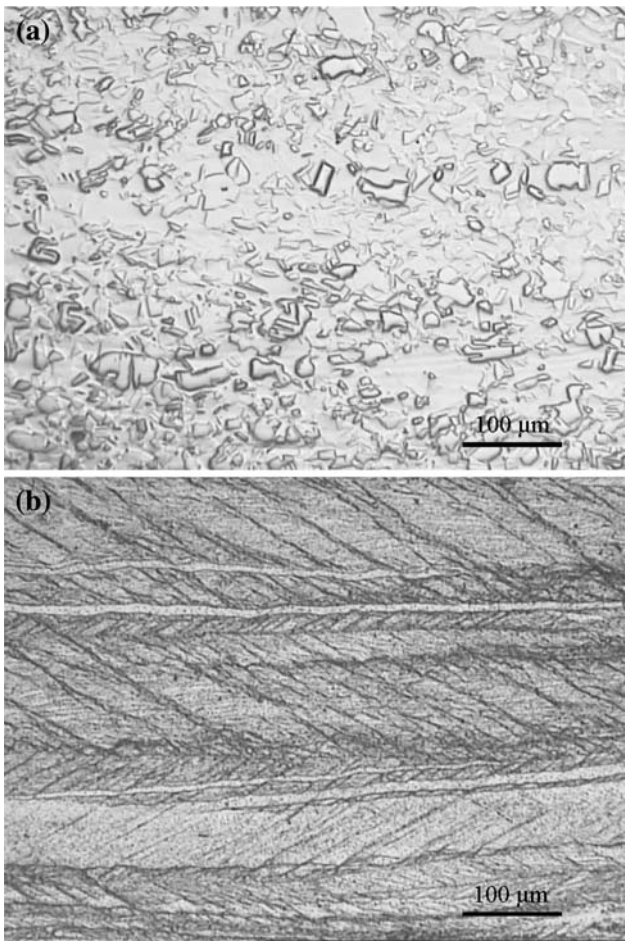

Fig. 6 Optical micrographs of the Cu–10Ni–20Zn alloy (**a**) and the Cu–10Ni–20Zn–1.2Al alloy (**b**) with 80% reduction aged at 450 °C

in equiaxed grains. The optical microstructures of the cold-rolled Cu–10Ni–20Zn–1.2Al and Cu–10Ni–20Zn alloys with 80% reduction after aging at 450 °C for 16 h are shown in Fig. 6. It can be seen that the microstructure of the Cu–10Ni–20Zn alloy consists mainly of recrystallized grains, and no precipitate particles are observed (Fig. 6a), which indicates that it only under goes recrystallization and the recrystallization was ultimately completed in the alloy. For the Cu–10Ni–20Zn–1.2Al alloy (Fig. 6b), the dislocation cell structure due to heavy deformation still remains and the recrystallization cannot be observed, and the grains that are filled with evenly distributed secondary-phase particles are elongated along the rolling direction. The suppression of recrystallization is likely due to the high density of small precipitates that effectively act as obstacles to dislocation and boundary migration [11]. It is well known that both the recovery and the recrystallization are accompanied by not only the rearrangement and annihilation of the dislocations, but also by the boundary movement and the cell growth. Therefore, the recrystallization process will be delayed in the cold-rolled Cu–10Ni–20Zn–1.2Al alloy where coherent precipitate particles have already precipitated. The same phenomena seem to operate in the Al–Cu alloys [11] and Cu–Ni–Al alloys [4].

The above data certainly show that a high density of small precipitates is present in the aged Cu–10Ni–20Zn–1.2Al alloy. However, a detailed analysis using TEM is necessary to characterize the size, shape, and distribution of the precipitates. The TEM images and the corresponding selected area electron diffraction (SAED) patterns, obtained from $[011]_m$ zone axis, of the solution treated Cu–10Ni–20Zn–1.2Al alloy in different conditions are shown in Fig. 7. At the earlier stage of aging, which corresponds to an under-aged condition, the bright-field image (Fig. 7a) reveals fine precipitates with high density in the matrix. The size of the precipitates is 4–8 nm at this aging stage. Precipitate particles are spherical and uniformly distributed, and the misfit strain caused by formation of the precipitates is not large. When the solution-treated Cu–10Ni–20Zn–1.2Al alloy was aged for 16 h, which corresponds to a peak-aged condition, the dark-field image (Fig. 7b) reveals fine precipitates spread uniformly in the matrix. The size of the precipitates is 6–12 nm at this aging stage. When aged at 500 °C for 128 h, corresponding to an over-aged condition, as shown in Fig. 7c, the precipitates were coarsened markedly and the density of precipitates is considerably lower than that in under-aged and peak-aged conditions. Precipitate particles are sheet-like and uniformly distributed. The corresponding indexed selected area electron diffraction (SAED) patterns along the $[011]_m$ zone axis allow to prove that the precipitates have a cube-on-cube orientation relationship with the matrix, and have an ordered lattice similar to the $L1_2$ type and structure parameters similar to those of the α-Cu matrix. Their habit planes were determined to {011} α-Cu planes of the surrounding α-Cu matrix, and an orientation relationship of $[011]_p//[011]_m$ and $(100)_p//(200)_m$ between the precipitates and the α-Cu matrix exists. The SAED patterns along the $[011]_m$ zone axis change little, but the diffraction spots resulting from precipitates become more and more visible with the aging time.

The dislocation density at different stages of aging for the cold-rolled alloy is characterized using the broadening of the matrix diffraction peaks by X-ray diffraction line profile analysis [12]. According to the optical microstructures of the cold-rolled Cu–10Ni–20Zn–1.2Al alloy, which shows no obvious recrystallization, change in dislocation density along each crystallographic plane during aging treatment can be estimated by examining the change in the full width at half maximum (FWHM) of the corresponding diffraction peak. The FWHM of the (111) and (220) matrix diffraction peak is plotted as a function of aging time at 450 °C in Fig. 8. From the figure, it can be seen that, the FWHM of diffraction peaks (111) and (220) is relatively

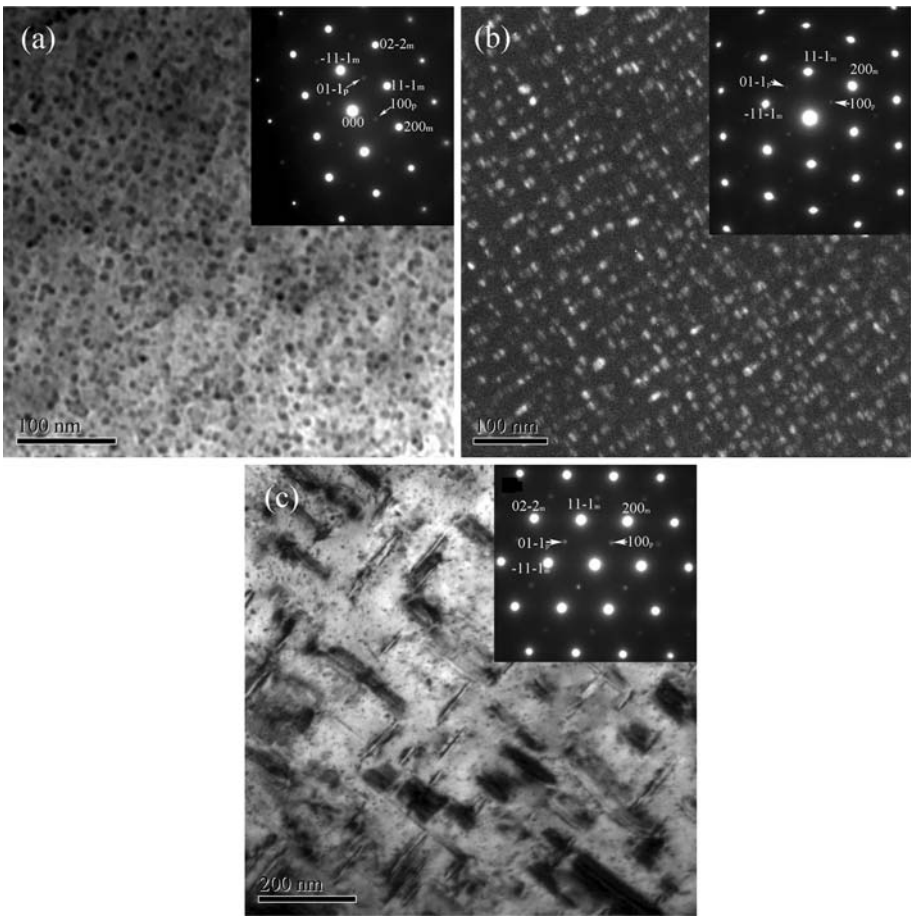

Fig. 7 Transmission electron micrographs and corresponding selected area electron diffraction (SAED) patterns, obtained from the $[011]_m$ zone axis, of the solution-treated Cu–10Ni–20Zn–1.2Al alloy aged at 450 °C for different times: **a** 1 h, bright-field image; **b** 16 h, dark-field image showing precipitates; **c** 128 h, bright-field image showing coarsened precipitates

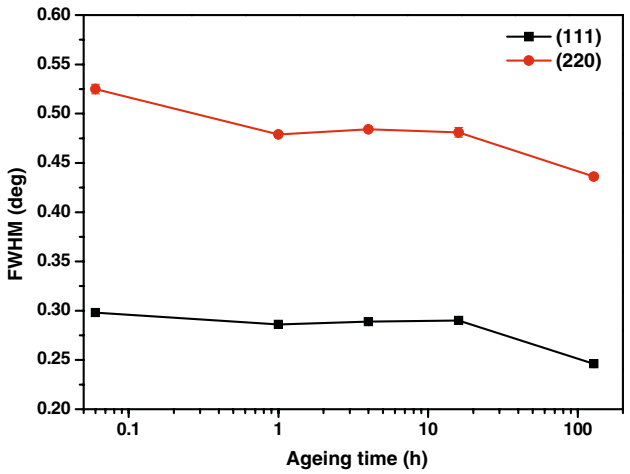

Fig. 8 The FWHM of the (111) and (220) matrix diffraction peak as a function of aging time at 450 °C

large in cold-rolled condition, decreases in the earlier stage of aging, and keeps stable until aging for 16 h, and then tend to decrease. It indicates that, in the cold-rolled Cu–10Ni–20Zn–1.2Al alloy, the dislocation density decreases in the earlier stage of aging due to recovery. On the other hand, due to a size misfit between precipitates and the surrounding matrix, the misfit strain caused by the formation of the precipitate during aging, which increases the dislocation density, increases with aging time until the precipitation process was completed. After aging for 1 h, the dislocation density changes a little during aging for up to 16 h, due to the effect of both the recovery and the misfit strain caused by the formation of precipitates. When the aging time is more than 16 h, the precipitation process was completed, the effect of recovery dominates and the dislocation density decreases with aging time.

During the solution treating and quenching treatments, the solute atoms like Al were dissolved in the matrix and retained in a metastable state. When the quenched material was isothermally aged, the clusters of the metastable solutes will occur with the vacancies. These fine clusters (precipitates) can act as a barrier for the dislocation movement, thus causing an enhancement of the initial strength. The hardness in the solution-treated Cu–10Ni–20Zn–1.2Al alloy increases with the aging time up to 16 h, and the aging process produces a fine distribution of nanosized precipitates. The increase in hardness observed during the aging of the solution-treated alloy with aluminum addition, as well as the rare change in hardness observed during the aging of the solution-treated alloy

without aluminum addition, clearly indicates that the nanosized precipitates result in the strengthening. Hence, the hardening mechanism during the isothermal aging treatment in the solution-treated Cu–10Ni–20Zn–1.2Al alloy should arise from precipitation hardening, since the strain hardening and recrystallization processes are believed not to occur in that case.

According to the effect of aluminum on the age-hardening behavior characterized by the hardness measurements, the hardness is raised from 58 Hv for the Cu–10Ni–20Zn alloy to 269 Hv for the peak-aged Cu–10Ni–20Zn–1.2Al alloy with 80% reduction. The strengthening mechanism, such as the work hardening and the precipitation hardening [13], are likely to apply to the precipitation hardened Cu–Ni–Zn–Al alloy studied in the present work. The hardness of Cu–10Ni–20Zn–1.2Al has been considerably improved under the same aged conditions after application of cold work to the solution-treated material. This has two possible reasons, i.e., (1) the presence of the precipitate particles refines the deformation microstructure and retains a higher dislocation density during deformation, and (2) the presence of a higher quantity of solutes in the matrix retards the recovery [4]. The interaction of the dislocations with the strain field of the coherent precipitates (precipitation hardening) and the cutting of the ordered precipitates by the dislocations (work hardening) are the main strengthening mechanisms, and the strength can be increased further by a higher precipitate density resulting from a heavy deformation [14].

On the other hand, the strength gradually decreases as the aging time increases in the cold-rolled Cu–10Ni–20Zn alloy, which arises from the recrystallization accompanying reduction of the work hardening effect. However, the strength will gradually decrease as the aging time increases further after peak aged in the solution-treated and cold-rolled Cu–10Ni–20Zn–1.2Al alloys, which arises from the coarse precipitation particles and/or the recrystallization.

Conclusions

The effect of aluminum on the precipitation hardening of the Cu–10Ni–20Zn alloy was investigated at different aging temperatures and times. Based on the above studies, we can draw the following conclusions:

(1) An addition of 1.2 wt% aluminum can increase the peak hardness from 58 Hv for the solution-treated Cu–10Ni–20Zn alloy to 185 Hv for the solution-treated Cu–10Ni–20Zn–1.2Al alloy during isothermal aging at 500 °C due to precipitation hardening.

(2) Cold work prior to the aging can further increase the hardness considerably under both the solution-treated and the peak-aged conditions. The value of hardness for the cold-rolled Cu–10Ni–20Zn–1.2Al alloy with 80% reduction reaches 269 Hv after aging at 400 °C for 64 h. The main strengthening mechanisms in this case can be attributed to the interaction of the dislocations with the strain field of the nanosized precipitates and the cutting of the ordered precipitates by the dislocations.

(3) The yield and tensile strengths of the cold-rolled Cu–10Ni–20Zn–1.2Al alloy with 80% reduction after aging at 450 °C for 8 h are 889 and 918 MPa, respectively, and the corresponding electrical conductivity reaches 10.96% IACS. The above properties are much higher than those of the alloy without aluminum and comparable to those of the Cu–Be alloys (C17200 and C17510) and the Cu–2.7Ti alloy.

(4) Formation of nanosized precipitates with high density results in precipitation hardening. The precipitates have a similar structure of the $L1_2$-type ordered lattice with their parameters close to those of the α-Cu matrix. The habit planes of the precipitates were determined to {011} α-Cu planes of the surrounding α-Cu matrix. It was found that an orientation relationship of $[011]_p//[011]_m$ and $(100)_p//(200)_m$ exists between the precipitates and the α-Cu matrix.

References

1. Metals handbook, properties and selection: non-ferrous alloys and special purpose materials, vol 2, 10th edn. ASM International, Metals Park, OH, 1990
2. Nagarjuna S, Srinivas M, Sharma KK (2000) Acta Mater 48:1807
3. Sierpiński Z, Gryziecki J (1999) Mater Sci Eng A 264:279
4. Cho Y-R, Kim Y-H, Lee TD (1991) J Mater Sci 26:2879. doi:10.1007/BF01124816
5. Zelaya E, Tolley A, Condó AM, Fichtner PFP (2007) Mater Sci Eng A 444:178
6. Zelaya E, Tolley A (2003) Scripta Mater 49:373
7. Lelatko J, Morawiec H (1996) J Mater Sci 31:2767. doi:10.1007/BF00687313
8. Murray JL (1997) In: Baker H, Okamoto H (eds) Alloy phase diagrams, ASM handbook. ASM International, Materials Park, OH, p 3.12
9. Dutta B, Pamiere EJ, Sellars CM (2001) Acta Mater 49:785
10. Nagarjuna S, Balabubramanian K, Sarma DS (1999) J Mater Sci 34:2929. doi:10.1023/A:1004603906359
11. Gorelik SS (1981) Recrystallization in metals and alloys. Mir publishers, Moscow, pp 379–413
12. Ungár T, Borbély A (1996) Appl Phys Lett 69:3173
13. Stranik MJ, Wang SC (2003) Acta Mater 51:5131
14. Čížek J, Procházka I, Smola B, Stulíková I, Očenášek V (2007) J Alloy Compd 430:92